Rolling blackout is required for bulk endocytosis in non-neuronal cells and neuronal synapses

Niranjana Vijayakrishnan, Elvin A. Woodruff III and Kendal Broadie*

Department of Biological Sciences, Vanderbilt Brain Institute, Vanderbilt University, Nashville, TN 37235, USA

*Author for correspondence (e-mail: kendal.broadie@vanderbilt.edu)

Accepted 2 October 2008
Journal of Cell Science 122, 114-125 Published by The Company of Biologists 2009
doi:10.1242/jcs.036673

Summary

Rolling blackout (RBO) is a *Drosophila* EFR3 integral membrane lipase. A conditional temperature-sensitive (TS) mutant (*rbo*^{ts}) displays paralysis within minutes following a temperature shift from 25°C to 37°C, an impairment previously attributed solely to blocked synaptic-vesicle exocytosis. However, we found that *rbo*^{ts} displays a strong synergistic interaction with the Syntaxin-1A TS allele *syx*$^{3\text{-}69}$, recently shown to be a dominant positive mutant that increases Syntaxin-1A function. At neuromuscular synapses, *rbo*^{ts} showed a strong defect in styryl-FM-dye (FM) endocytosis, and *rbo*^{ts};*syx*$^{3\text{-}69}$ double mutants displayed a synergistic, more severe, endocytosis impairment. Similarly, central *rbo*^{ts} synapses in primary brain culture showed severely defective FM endocytosis. Non-neuronal nephrocyte Garland cells showed the same endocytosis defect in tracer-uptake assays. Ultrastructurally, *rbo*^{ts} displayed a specific defect in tracer uptake into endosomes in both neuronal and non-neuronal cells. At the *rbo*^{ts} synapse, there was a total blockade of endosome formation via activity-dependent bulk endocytosis. Clathrin-mediated endocytosis was not affected; indeed, there was a significant increase in direct vesicle formation. Together, these results demonstrate that RBO is required for constitutive and/or bulk endocytosis and/or macropinocytosis in both neuronal and non-neuronal cells, and that, at the synapse, this mechanism is responsive to the rate of Syntaxin-1A-dependent exocytosis.

Key words: Syntaxin, Shibire, Synaptic vesicle, Endosome, Neuromuscular junction, Garland cell, Primary neuron culture

Introduction

Neuronal synapses efficiently couple neurotransmitter release with compensatory mechanisms that recycle the fusion-competent synaptic vesicle (SV) pool. Two full-fusion pathways mediate SV recovery: direct clathrin-mediated endocytosis (CME) of SVs (Heuser and Reese, 1973; Slepnev and De Camilli, 2000), and bulk retrieval and/or macroendocytosis of large portions of membrane to form endosomes (Leenders et al., 2002; Marxen et al., 1999; Takei et al., 1996). SVs that are internalized via CME may immediately enter the fusion-competent pool or fuse with sorting endosomes prior to rebudding (Hinshaw, 2000; Koenig and Ikeda, 1989; Narita et al., 1989; Wenk and De Camilli, 2004). Under high-demand conditions, synapses use the bulk-plasma-membrane-retrieval mechanism in parallel with CME (Holt et al., 2003; Richards et al., 2000). This activity-dependent formation of endosomes was first demonstrated in central brain synapses (Takei et al., 1996) and subsequently in many diverse synapses, including in *Drosophila* neuromuscular junctions (NMJs) (Heerssen et al., 2008; Koenig and Ikeda, 1996; Kuromi and Kidokoro, 1998), frog NMJs (Richards et al., 2000), goldfish retinal bipolar synapses (Holt et al., 2003; Neves et al., 2001) and mammalian Calyx of Held synapses (de Lange et al., 2003). Bulk endocytosis commences within 1-2 seconds of strong stimulation (Leenders et al., 2002; Marxen et al., 1999; Teng et al., 2007), but very little is known about the molecular mechanisms involved. Synaptic bulk endocytosis has often been compared to macropinocytosis in non-neuronal cells; the process is similarly sensitive to disruption of the actin cytoskeleton and requires activation of Rho GTPases (Holt et al., 2003; Richards et al., 2004).

We report here the characterization of a new player with a specific role in bulk endocytosis; Rolling blackout (RBO; also known as EFR3, Pho eighty-five requiring 3 and STMA). We previously reported that conditional temperature sensitive (TS) *rbo*^{ts} mutants manifest complete blindness and paralysis within minutes upon shift to restrictive temperature (Huang et al., 2004; Huang et al., 2006). RBO is a well-conserved integral plasma-membrane protein and predicted lipase (Vijayakrishnan and Broadie, 2006). In *rbo*^{ts} brain, phosphatidylinositol (4,5)-bisphosphate [PtdIns(4,5)P_2] accumulates and diacylglycerol (DAG) is concomitantly reduced within minutes upon shift to restrictive temperature. However, the exact RBO lipase substrate in the PtdIns(4,5)P_2-DAG pathway has not been identified, despite exhaustive attempts (Vijayakrishnan and Broadie, 2006). Our previous data pointed to RBO function in SV exocytosis, with vesicles accumulating within minutes at the restrictive temperature, being arrested at the docking stage at presynaptic active zones (Huang et al., 2006). Crucial to this model, we showed that *rbo*^{ts} displays a strong synergistic behavioral interaction with the *syntaxin-1A* TS allele *syx*$^{3\text{-}69}$ (T254I) (Littleton et al., 1998). Double-homozygous mutants paralyze at a lower temperature than either single mutant, suggesting that RBO and Syntaxin-1A act synergistically in SV exocytosis. However, a recently published analysis of *syx*$^{3\text{-}69}$ revealed that this allele is in fact a dominant positive mutation causing elevated Syntaxin-1A function (Lagow et al., 2007). This revelation forced us to question our hypothesis. We have therefore since performed many additional studies, with better tools and in multiple cell types, to assess the functional requirements for RBO in both neurons and non-neuronal cells.

In this study, we performed FM1-43 dye cycling assays both at the well-characterized NMJ and the novel setting of central synapses in primary culture. Both synapse classes display severely defective SV endocytosis in *rbo*^{ts} mutants. Nevertheless, ultrastructural analyses of synaptic boutons at rest and post-stimulation show an increase in SV density and accumulation of docked SVs in *rbo*^{ts}

synapses, similar to the results obtained in adult dorsal longitudinal muscle (DLM) synapse (Huang et al., 2006), posing us a conundrum. We therefore combined FM-dye-uptake experiments with photoconversion electron microscopy to reveal that loss of RBO function causes a specific blockade in the activity-dependent bulk-endocytosis generation of endosomes. We performed parallel fluid-phase tracer-uptake studies in non-neuronal Garland cells, a well-established constitutive endocytosis assay system (Dermaut et al., 2005; Kosaka and Ikeda, 1983). These studies similarly showed a complete arrest in macropinocytosis in *rbo*^{ts} mutants, comparable to the blockade that we observed in *shibire*^{ts} (*shi*^{ts}; Dynamin) mutants. Tracer ultrastructure studies in Garland cells also showed a complete loss of tracer uptake into endosomes. Together, these results show that RBO is specifically required for the bulk endocytosis pathway only, in both neuronal synapses and non-neuronal cells.

Results

RBO is required for endocytosis at the neuromuscular synapse

FM1-43 styryl lipophilic dye imaging was used to assay SV cycling at the larval NMJ (Fergestad and Broadie, 2001; Renden and Broadie, 2003; Trotta et al., 2004). Dye can be loaded by a depolarizing stimulus, triggering SV endocytosis, and then unloaded by a second depolarizing stimulus, triggering SV exocytosis. Dye-uptake and -release assays were performed at staged permissive (25°C) and restrictive (37°C) temperatures to independently examine the effects on endocytosis and exocytosis. Four genotypes were assayed under both conditions: wild-type control (Oregon-R; OR), *rbo*^{ts} and *syx*$^{3-69}$ single mutants, and the *rbo*^{ts};*syx*$^{3-69}$ double-homozygous mutant (Fig. 1).

Fig. 1A shows a schematic of the two assays employed. To test the predicted roles of RBO and Syntaxin-1A in SV exocytosis, FM dye was loaded with a 60 mM [K^+] stimulus for 2 minutes at the permissive 25°C condition, and then shifted to the restrictive 37°C for 10 minutes prior to applying a second depolarizing stimulus (Fig. 1A, protocol 1). Under these conditions, the *rbo*^{ts} and *syx*$^{3-69}$ single mutants showed dye loading comparable to the wild-type control (P=0.98 comparing *rbo*^{ts} with wild type) (Fig. 1B). By contrast, *rbo*^{ts};*syx*$^{3-69}$ double mutants showed a strong dye-loading defect even at this permissive temperature (Fig. 1B, bottom panel). Quantification of this phenotype revealed a very highly significant (P<0.0001) decrease in FM endocytosis in the double mutant only [fluorescence intensities: OR, 64.49±0.96 (n=4); *syx*$^{3-69}$, 63.39±2.58 (n=6); *rbo*^{ts}, 64.31±5.36 (n=5); and *rbo*^{ts};*syx*$^{3-69}$, 28.81±2.17 (n=11)] (Fig. 1D).

In protocol 2 (Fig. 1A), FM dye was loaded in the restrictive 37°C condition and then shifted to permissive 25°C for 10 minutes prior to applying the second depolarizing stimulus. Under these conditions, *syx*$^{3-69}$ continued to load similarly to wild type, showing no requirement for Syntaxin-1A in endocytosis (Fig. 1C,D, right). By contrast, *rbo*^{ts} showed a very significant (P<0.0001) impairment (Fig. 1C). The mutant took up ~50% less dye than wild-type controls [fluorescence intensities: OR, 79.07±1.28 (n=9); *rbo*^{ts}, 40.63±3.07 (n=11)] (Fig. 1D, right). A wild-type copy of *rbo* in the mutant background completely rescued this loading defect [77.01±1.81 (n=6)] (Fig. 2). The *rbo*^{ts};*syx*$^{3-69}$ double mutant also showed a severe defect in FM endocytosis; however, the defect at 37°C and 25°C was comparable, suggesting that the interaction was already maximal at the permissive temperature [*rbo*^{ts};*syx*$^{3-69}$, 32.18±2.85 (n=8), compared with OR; P<0.0001] (Fig. 1D, right). Because the double mutant showed such poor loading at 2 minutes, a longer 5-minute load was used to determine whether unloading was defective (Fig. 1C, bottom panel). The amount of dye loaded remained significantly reduced (P=0.0064), but the relative amount of dye unloaded was not significantly different (P=0.10) in the double mutant compared with wild type (OR, 43.64%; *rbo*^{ts};*syx*$^{3-69}$, 55.63%). Together, these data indicate that RBO has a crucial role

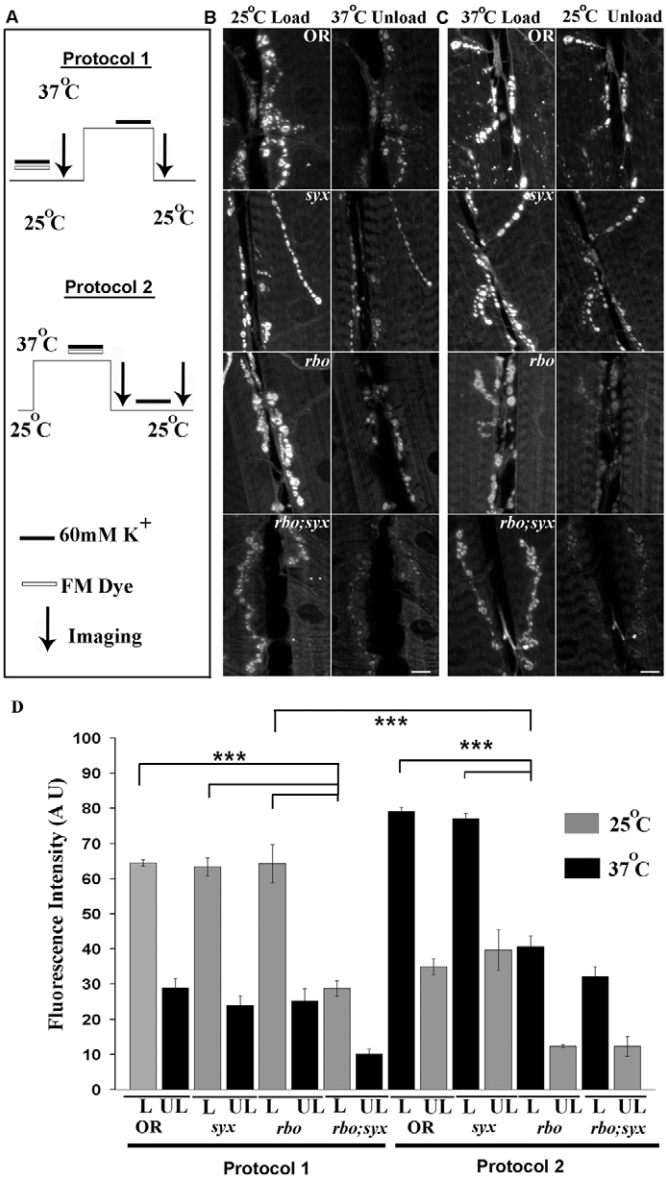

Fig. 1. RBO facilitates FM1-43-dye endocytosis at the neuromuscular synapse. (A) Schematic of dye-loading, temperature and imaging protocols used at the larval NMJ. In protocol 1, FM1-43 was loaded for 2 minutes with 60 mM [K^+] at 25°C and then unloaded for 2 minutes with 60 mM [K^+] at 37°C. In protocol 2, following a 10-minute incubation at 37°C, dye was loaded for 2 minutes at 37°C and then unloaded for 2 minutes at 25°C. (B) Representative images of wild type (OR), *syx*$^{3-69}$ and *rbo*^{ts} single mutants, and the *rbo*^{ts};*syx*$^{3-69}$ double mutant following protocol 1. (C) Top three panels show representative images comparing FM1-43 loading and unloading following protocol 2. Bottom panel shows *rbo*^{ts};*syx*$^{3-69}$ 37°C unloading after 5 minutes of loading at 25°C. Scale bars: 10 µm. (D) Quantification of loading (L) and unloading (UL) with both protocols. Error bars show mean ± s.e.m. ***Significance of P<0.001.

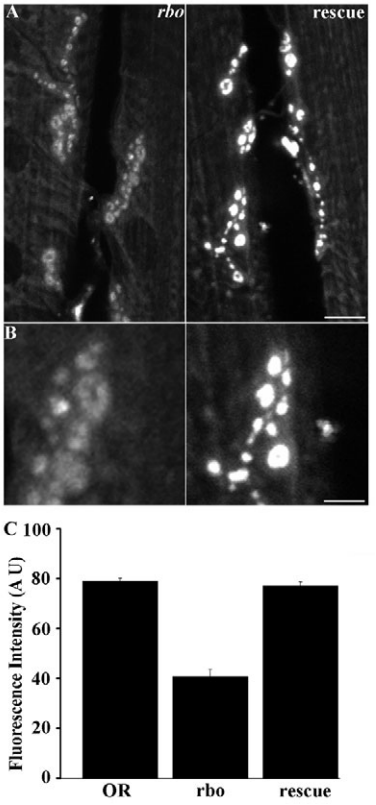

Fig. 2. Endocytic defects in *rbo*^{ts} mutants are fully rescued by the wild-type *rbo* gene. (A) Representative images of *rbo*^{ts} and *rbo*^{ts}/*rbo*^{2}; *rbo-egfp*/*rbo-egfp* (rescue) larval NMJs loaded with FM1-43 dye after 10 minutes at 37°C (see Fig. 1, protocol 2). Scale bar: 10 µm. (B) Magnified loaded synaptic boutons in both genotypes. The wild-type *rbo* transgene rescues the *rbo*^{ts} dye-loading defect. Scale bar: 5 µm. (C) Quantification of dye loading in wild-type (OR) and *rbo*^{ts} compared with rescue animals.

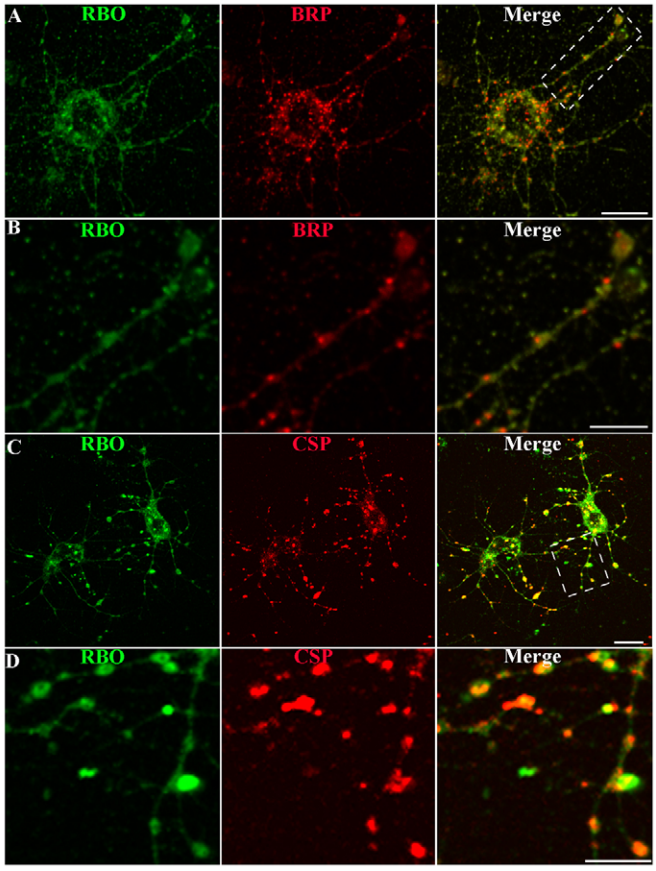

Fig. 3. RBO localizes to synapses in central brain primary neuron cultures. Representative images of neuron cultures of *rbo*^{2}/*rbo*^{2}; *rbo-egfp*/*rbo-egfp*. (A) RBO-GFP (green) at 6 DIV, double-labeled with anti-BRP (red) marking active zones. Scale bar: 10 µm. (B) Area in boxed area in A magnified to show RBO-GFP and BRP colocalization in axonal synaptic varicosities. Scale bar: 5 µm. (C) RBO-GFP (green) double-labeled with anti-CSP (red) marking synaptic punctae. Scale bar: 10 µm. (D) Area in boxed area in C magnified to show RBO-GFP and CSP colocalization in synaptic punctae. Scale bar: 5 µm.

in endocytosis that is exacerbated by the elevated SV cycling driven by the *syx*$^{3\text{-}69}$ mutant.

RBO is required for endocytosis in central brain synapses

There appeared to be a disparity between our previous results at the adult DLM synapse, which suggest a role for RBO in SV exocytosis (Huang et al., 2006), and our new results at the larval NMJ synapse. Consistently, *rbo*^{ts} at restrictive temperature displays a total blockade of neurotransmission within 3 minutes at the adult DLM synapse, whereas there is no functional block at the larval NMJ (Huang et al., 2006). One possible explanation is that RBO displays a developmental-stage-specific (larval vs adult) or synapse-type-specific differential requirement. To test these possibilities, we wished to perform comparable FM1-43 experiments in a range of synapses. The DLM synapse is not accessible for FM dye assays (Beramendi et al., 2007). We therefore turned to primary neuronal cultures derived from the late-stage pupal brain, using methods pioneered by Jiang et al. (Jiang et al., 2005). This technique gives excellent access to a large set of diverse central brain synapses (Figs 3 and 4).

We sought first to determine whether RBO is expressed in primary-culture neurons. We cultured disassociated central brain neurons from *rbo*-null mutants rescued to adulthood by an *rbo-egfp* transgene under native *rbo* promoter control (Fig. 3). RBO-GFP expression was assayed using anti-GFP antibody staining. At the pupal brain dissection period (~55-70 hours after puparium formation), RBO expression was clearly visible in the brain, where the protein is tightly restricted to the synaptic neuropil (data not shown). In individual disassociated brain neurons at 6 days in vitro (DIV), anti-GFP labeling similarly showed clear RBO expression (Fig. 3A). In neurons that were double-labeled with the presynaptic marker anti-Bruchpilot (BRP), an overlapping punctate pattern was observed, very similar to that reported by Oh et al. (Oh et al., 2008). RBO expression was clearly observed in varicosities along axonal processes, colocalized with BRP and Cysteine string protein (CSP) in synapses (Fig. 3B-D). These same varicosities have been recently shown to be presynaptic specializations by ultrastructural criteria (Oh et al., 2008). These data show that RBO is expressed in synapses, colocalizing with presynaptic markers in central brain neurons.

It has been recently shown that these primary-culture neurons develop mature electrophysiological properties, express ligand-gated neurotransmitter receptors and form functional synaptic contacts indicative of a functional SV-release machinery (Campusano et al., 2007; Jiang et al., 2005; Su and O'Dowd, 2003). However, to the best of our knowledge, presynaptic-vesicle cycling has not been

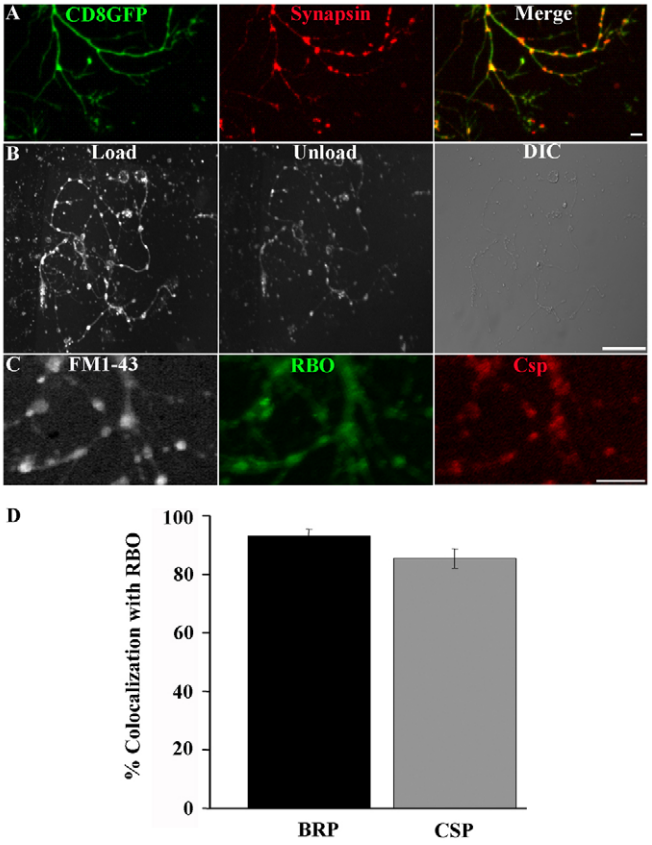

Fig. 4. RBO localizes to functional synapses with cycling SVs. (A) Cultured neurons containing *elav*-GAL4 driven UAS-CD8::GFP (green) double-labeled with anti-Synapsin (red) to show axonal varicosities containing the presynaptic marker. Scale bar: 2 µm. (B) FM1-43 labeling with 60 mM [K^+] for 45 seconds loads synaptic varicosities (left). A shorter, 30 second, exposure to 60 mM [K^+] partially unloads dye (middle). Nomarski DIC image showing neuronal structure (right). Scale bar: 20 µm. (C) In rbo^2/rbo^2; *rbo-egfp*/*rbo-egfp* 6-DIV cultures, loaded FM1-43 dye (white) colocalizes with RBO-GFP (green) and the synaptic marker anti-CSP (red). Scale bar: 5 µm. (D) Quantification of the percentage of colocalization of BRP and CSP with RBO-GFP punctae.

directly demonstrated in this system (Kuppers-Munther et al., 2004). We therefore next sought to determine whether the presumed synaptic varicosities along axonal processes take up and release FM dye in a depolarization-dependent manner. Neurons were labeled with the membrane marker CD8-GFP, to reveal varicosities, and synaptic markers, including anti-Synapsin (Fig. 4A). FM1-43 dye cycling was stimulated with depolarizing high-[K^+] saline, as was performed at the NMJ synapse. FM dye was taken into the stimulated axonal varicosities (Fig. 4B, load). Following a second depolarizing stimulus, the loaded FM dye was effectively released again (Fig. 4B, unload). Neurons were labeled with FM1-43, imaged live and subsequently fixed and stained for RBO and synaptic markers such as CSP (Fig. 4C). Active synapses clearly localized RBO with other synaptic markers. Quantification of the percentage of BRP- or CSP-positive synapses that co-express RBO showed 93.09±2.31% and 85.48±3.36% overlap, respectively (Fig. 4D). Taken together, these data show that RBO is localized to functional presynaptic varicosities.

We therefore performed FM1-43 dye imaging studies to examine the role of RBO in SV cycling in central synapses. To test the restrictive condition, cultured control and rbo^{ts} neurons were incubated for 10 minutes at 37°C in Ca^{2+}-free saline, after which a 45-second pulse of FM1-43 was applied in depolarizing high-[K^+] saline (Fig. 5). In wild-type (OR) neurons, some cell-body dye loading was evident, but most of the dye was endocytosed into the synaptic varicosities along axon processes (Fig. 5A,B, right, arrows). By sharp contrast, rbo^{ts} neurons displayed greatly reduced endocytosis. The majority of mutant neurons loaded poorly, with faintly detectable fluorescent puncta (Fig. 5C), and a subset showed almost no detectable loading (Fig. 5D). A wild-type copy of *rbo* in the mutant background rescued dye loading (Fig. 5E), proving that the *rbo* mutation is responsible for this endocytosis defect. To quantify this phenotype, culture fields were selected blind to fluorescence using Nomarski optics and the number of FM1-43-loaded synaptic puncta per 20-µm length of axonal process was then counted and calculated as the percentage of total varicosities. This blind quantification showed a very highly significant (P<0.0001) decrease in dye loading in rbo^{ts} mutants compared with control (OR, 80.25±3.74; rbo^{ts}, 39.48±3.68; and rescue, 77.37±2.66) (Fig. 5F). These results demonstrate that a strikingly similar rbo^{ts} endocytosis defect is shared between larval neuromuscular synapses and pupal central brain synapses. We therefore set out to further investigate the basis of this endocytosis requirement.

RBO is required for endocytosis in non-neuronal cells

Garland or 'wreath' cells, involved in rapid fluid-phase endocytic uptake from the hemolymph, are a long-established system used to elucidate mechanistic requirements during endocytosis (Kosaka and Ikeda, 1983; Narita et al., 1989). Several synaptic endocytic mutants show defects in tracer and/or dye uptake in Garland cells (Chang et al., 2002; Dermaut et al., 2005; Lloyd et al., 2002). Because these cells are much larger than synaptic boutons, they provide excellent visualization of endocytic defects and allow dysfunction to be pin-pointed with greater accuracy. To test whether rbo^{ts} mutants and rbo^{ts};$syx^{3\text{-}69}$ double mutants have a more generalized endocytic defect, we performed Texas-red–avidin (TR-avidin)-uptake experiments on Garland cells (Fig. 6).

RBO expression was clearly detected in Garland cells (Fig. 6A). The protein is primarily localized to the plasma membrane, as at the synapse (Vijayakrishnan and Broadie, 2006). In addition, RBO was also present in a small subset of internal organelles (Fig. 6B, arrows). Following application of TR-avidin tracer for 5 minutes at 25°C, internalized vesicles were observed in the cell periphery in both wild type (Fig. 6C) and rbo^{ts} (Fig. 6D). At this permissive temperature, rbo^{ts} cells were indistinguishable from wild type in the number and distribution of endocytosed vesicles. Fluorescence intensity underlying the plasma membrane was similar in all genotypes (OR, 51.33±5.73; rbo^{ts}, 43.00±3.86; rbo^{ts};$syx^{3\text{-}69}$, 44.96±4.00; shi^{ts}, 42.71±1.54) (Fig. 6G). At the restrictive 37°C, wild-type cells similarly displayed a large number of well-internalized vesicles (61.56±2.88) (Fig. 6C, right). By sharp contrast, no TR-avidin-positive vesicles were observed in rbo^{ts} cells following a 10-minute incubation at 37°C, indicating an essentially complete block in endocytosis (Fig. 6D, right). The rbo^{ts};$syx^{3\text{-}69}$ cells similarly took up dye at permissive temperature and showed the same profound endocytosis block at the restrictive temperature (rbo^{ts}, 5.48±1.67; rbo^{ts};$syx^{3\text{-}69}$, 6.80±2.3; n=12) (Fig. 6E,G). TS *shibire* (shi^{ts}) Dynamin mutant cells, used as a positive control and a known comparison, showed a similar endocytosis-block profile (shi^{ts}, 7.38±0.576; n=12) (Fig. 6E,G). These results suggest that RBO is essential for endocytosis.

To precisely characterize the defect in *rbo*^{ts} mutants, we performed ultrastructural analyses (Fig. 7). Garland cells were seen to possess tubular invaginations of the plasma membrane extending ~3 μM into the interior (labyrinthine channels) (Fig. 7, arrows) and numerous endosomal α vacuoles (labeled a in Fig. 7). At 25°C, *rbo*^{ts} cells appeared indistinguishable from wild-type cells in all respects (Fig. 7A). By stark contrast, dramatic endocytic changes were observed in *rbo*^{ts} mutants following upshift for just a few minutes from 25°C to restrictive 37°C. The labyrinthine channels became elongated and drastically engorged in *rbo*^{ts} at 37°C, compared with mutants at 25°C or wild type at either temperature (Fig. 7B). In the mutant, vacuolar structures developed within the engorged channels. In *shi*^{ts} mutants at 37°C, labyrinthine channels similarly elongated and accumulated irregular pits as a result of failure to pinch off membrane from the surface (Kosaka and Ikeda, 1983; Narita et al., 1989). These common defects suggest that this *rbo*^{ts} phenotype arises from a block of endocytosis from labyrinthine-channel plasma membrane. At 37°C, *rbo*^{ts} cells also contain fewer endosomal α vacuoles, and the few that are present appear enlarged and of more irregular shape (Fig. 7C). These defects are consistent with a failure to form endosomes from the labyrinthine-channel plasma membrane following acute removal of RBO function.

Horseradish peroxidase (HRP) provides an excellent electron-microscopy tracer for endocytosis in Garland cells (Lloyd et al., 2002). Garland cells were dissected and incubated with HRP at 25°C or following a 10-minute incubation at 37°C (Fig. 8). At permissive temperature, HRP was clearly observed in the lumen and internal membrane of peripherally located large endosomal α vacuoles in both *rbo*^{ts} and wild-type cells (data not shown). However, when the number of endosomes was quantified, even at permissive temperature *rbo*^{ts} cells displayed a >50% decrease in HRP-labeled endosomes (Fig. 8E). Following 10 minutes at 37°C, wild-type cells clearly endocytosed HRP tracer into α vacuoles (Fig. 8A,B, left). By sharp contrast, almost no HRP was observed in *rbo*^{ts} endosomes (Fig. 8A,B, right), indicating a near complete block in endocytosis. The α vacuoles that were present in the mutant clearly were made under the permissive condition, as they never contained the HRP tracer. Consistent with an endocytic block, use of tannic acid (TA) as a label to impregnate membrane that was contiguous with the extracellular space, shows these labyrinthine channels to be abnormally elongated and ramified in *rbo*^{ts} mutants compared with controls (Fig. 8C). Quantification of cell area showed no change at 25°C but a highly significant increase in *rbo*^{ts} at 37°C (OR, 266±21 μm^2; *rbo*^{ts}, 345±33 μm^2; P=0.009). Area was significantly increased in *rbo*^{ts} mutants after the 10-minute temperature shift (25°C, 229±22 μm^2; 37°C, 345±33 μm^2; P=0.007) (Fig. 8D). Quantification of HRP-loaded endosomes per section shows a significant reduction in *rbo*^{ts} at 25°C (OR, 32±1.4; *rbo*^{ts}, 14±0.8; P=0.0001) and near complete loss at 37°C (OR, 28±6.8; *rbo*^{ts}, 0.2±0.14; P<0.0001) (Fig. 8E). These results show that RBO is essential in the endocytosis mechanism that generates endosomes.

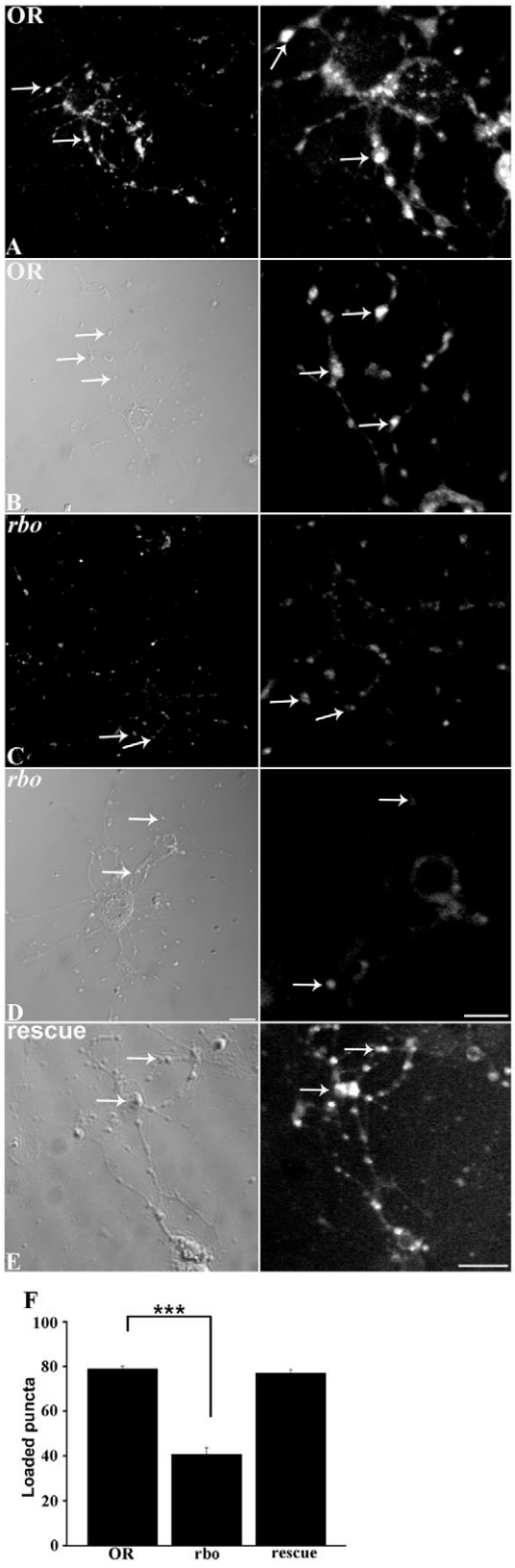

Fig. 5. RBO facilitates FM1-43-dye endocytosis in central brain synapses. Dye labeling in cultured neurons from wild type (OR) and *rbo*^{ts} after 10 minutes at 37°C. Left panels show lower-magnification fields and Nomarski DIC images; right panels show higher-magnification images of FM1-43-labeled synapses (arrows). (A-D) Shown is the range of loading in wild type with more intense (A) and less intense (B) labeling, and in *rbo*^{ts} with more intense (C) and less intense (D) labeling. (E) Rescue of loading in *rbo*^{ts}/*rbo*^{2}; *rbo-egfp*/*rbo-egfp* neurons. Scale bars: 10 μm. (F) Quantification of FM1-43 loading. The number of loaded varicosities as a percentage of the total varicosities from DIC images, per 20 μm of axon length. Error bars show mean ± s.e.m. for four independent trials for each genotype. ***Significance of P<0.001.

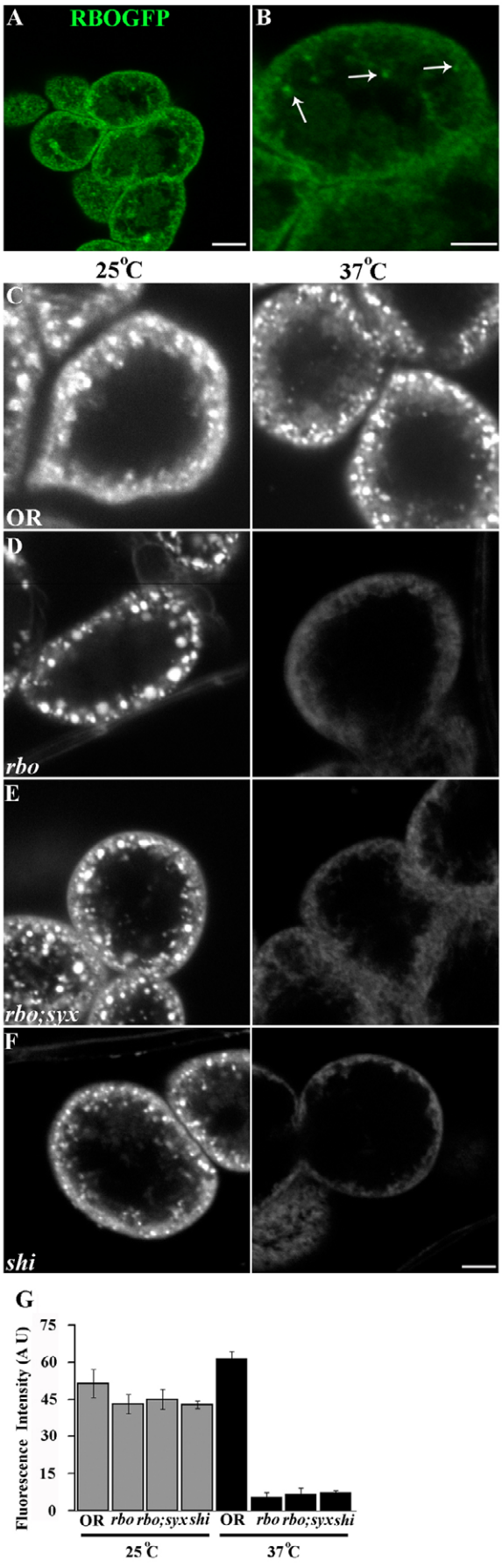

RBO is required for bulk endocytosis formation of endosomes at the synapse

The role of endosome trafficking at the synapse has long been controversial (Heuser and Reese, 1973; Takei et al., 1996; Teng et al., 2007). Based on the insights derived from the Garland-cell analyses, we formed the hypothesis that RBO might have a select function in a subset of the endocytosis pathways, specifically the bulk endocytosis that forms endosomes. The functional defects observed at the larval NMJ based on our FM imaging studies (Figs 1 and 2) and our previous electrophysiological studies (Huang et al., 2006) also appear consistent with a role for RBO in the bulk-endocytosis pathway. To test this hypothesis, we performed ultrastructural experiments at the NMJ synapse, at rest and following stimulation (Fig. 9), and also using FM1-43 photoconversion to track different endocytosis pathways (Fig. 10).

Wild-type and *rbo*^{ts} boutons were indistinguishable based on any ultrastructural criteria in unstimulated synapses at the 25°C permissive temperature (data not shown). Following 10 minutes at 37°C, mutant and control boutons remained remarkably similar, although some slight changes in SV pools became apparent (Fig. 9A). The total number of vesicles per bouton profile in *rbo*^{ts} (250±32 SVs/bouton profile) appeared to be elevated compared with controls (200±23), although the increase was not quite statistically significant (Fig. 9C). In addition, there was a significant (P<0.05) increase in the number of SVs clustered at the presynaptic active zone (within 250 nm) (OR, 13.0±1.4; *rbo*^{ts}, 17.2±1.2) and closely docked at the T-bar (within 20 nm) (OR, 1.2±0.28; *rbo*^{ts} 2.3±0.33) (Fig. 9C). The unstimulated terminals also contained cisternae (>60 nm in diameter) that were presumed to be endosomes. The number of these structures did not differ significantly between *rbo*^{ts} and wild type after 10 minutes at 37°C (OR, 4.4±1.3; *rbo*^{ts}, 5.3±0.84). Thus, acute removal of RBO function leads to a relatively mild accumulation of SVs in the presynaptic bouton.

Synaptic ultrastructure was next assayed following depolarizing stimulation at 37°C [10- or 20-minute incubation with 60 mM [K^+] saline] (Fig. 9B). This condition is known to place a high demand on the SV cycle, driving high rates of exocytosis and endocytosis (see Figs 1 and 2). Stimulation eliminated the overall accumulation of SVs in *rbo*^{ts} mutants, but the elevated clustered and docked vesicle pools persisted under these conditions of intense demand (Fig. 9B,C). The number of clustered vesicles remained significantly elevated (OR, 10.5±0.60; *rbo*^{ts}, 16.6±1.1; P<0.01) and the number of docked vesicles also remained slightly greater (OR, 1.7±0.26; *rbo*^{ts}, 2.1±0.23). Importantly, as is characteristic of endocytic mutants of the direct SV pathway (Gonzalez-Gaitan and Jackle, 1997; Poodry and Edgar, 1979; Verstreken et al., 2003), significant vesicle depletion did not occur. The striking effect of high-[K^+] stimulation is the massive production of large (>60 nm) cisternae – endosomal-like organelles in control boutons (Fig. 9B, arrows). Although these structures exist in *rbo*^{ts} mutants at permissive temperatures, as expected because RBO

Fig. 6. RBO is required for Texas-red–avidin-tracer endocytosis in Garland cells. (A) RBO-GFP in *rbo*^{2}/*rbo*^{2}; *rbo-egfp*/*rbo-egfp* Garland cells is strongly expressed at the periphery. (B) Most RBO-GFP is tightly associated with the plasma membrane, but some RBO associates with internal organelles (arrows). (C) Wild-type (OR) cells loaded at 25°C (left) or following 10 minutes at 37°C (right). (D) *rbo*^{ts} at 25°C (left) is indistinguishable from control, but at 37°C (right) shows no dye internalization. (E) *rbo*^{ts};*syx*$^{3\text{-}69}$ also shows a complete block of uptake at 37°C. (F) As positive control, *shibire*^{ts} shows a block at 37°C (right); this phenotype is indistinguishable from *rbo*^{ts}. Scale bars: 5 µm. (G) Quantification of fluorescence intensity underlying the plasma membrane.

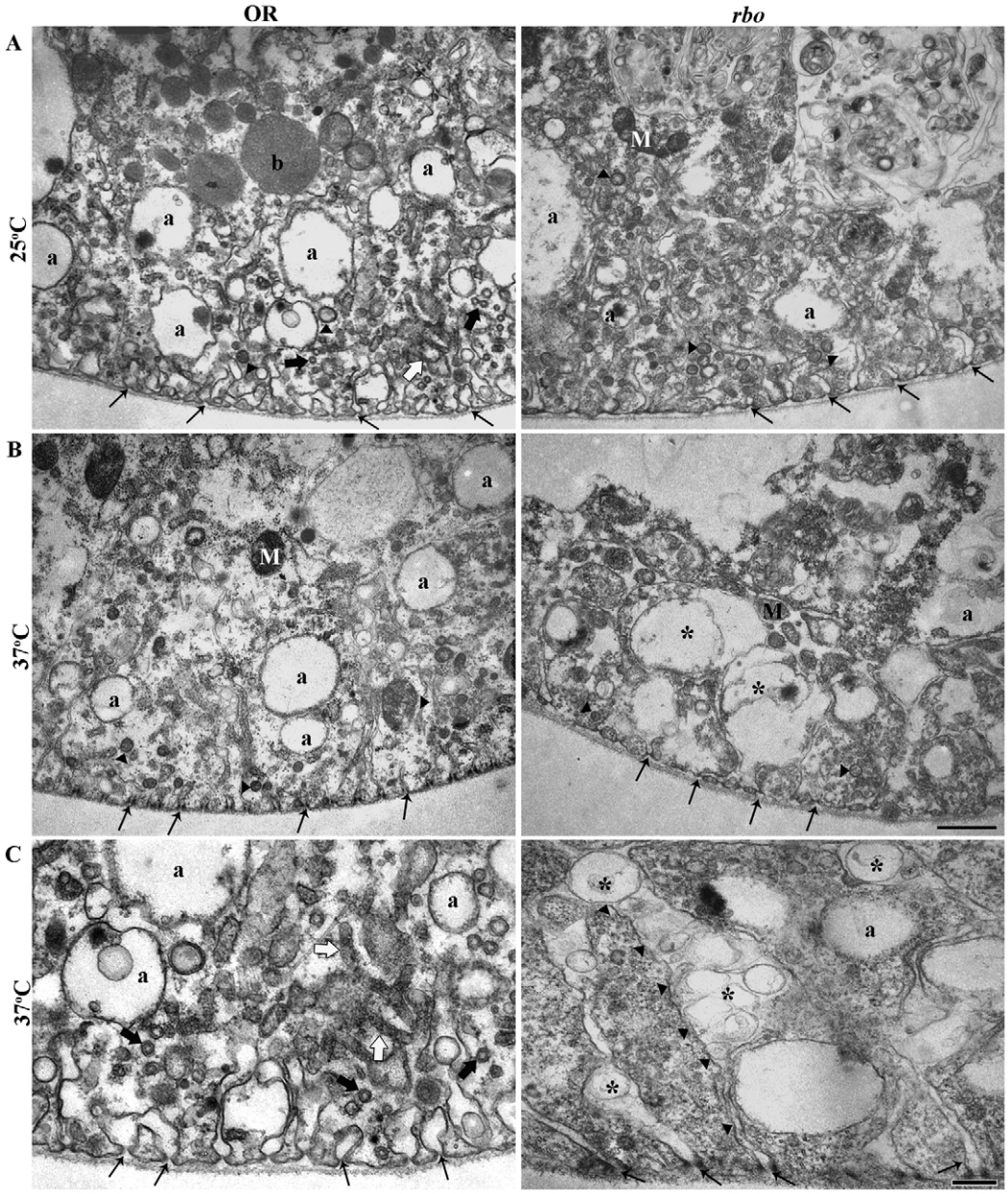

Fig. 7. Ultrastructure of Garland cells in wild type and in *rbo*^{ts} mutants. (A) Transmission electron microscopy (TEM) images of wild-type and *rbo*^{ts} Garland cells at 25°C. The cortical cell region extends ~3 μm, with many labyrinthine channels (thin black arrows). Numerous α vacuoles (a), longitudinal (white arrows) and transverse (thick black arrows) tubular elements, and coated vesicles and/or pits (arrowheads) are present in all section planes. Many sections also contain mitochondria (M) and β vacuoles (b). Wild type and *rbo*^{ts} appear indistinguishable at 25°C. (B) Following 10 minutes at 37°C, the number of α vacuoles in *rbo*^{ts} cells is reduced, with remnant vacuoles being larger and more irregular. Labyrinthine channels swell and distend with many vacuolar structures (*). Scale bar: 1 μm. (C) Higher-magnification images at 37°C. In *rbo*^{ts}, very elongated labyrinthine channels extend into the cell; these channels contain many vacuolar structures (*). Thin black arrows show the origin of the labyrinthine channels at the basement membrane. Scale bar: 250 nm.

is functional, stimulation in the absence of RBO function completely failed to induce the production of more cisternae (Fig. 9B, right). After 10 minutes at 37°C, wild-type synapses produced nearly fourfold more cisternae (at rest, 4.4±1.3; stimulated, 15.1±2.4), whereas *rbo*^{ts} synapses did not display any activity-dependent cisternae production (at rest, 5.3±0.84; stimulated, 3.25±0.56) (Fig. 9D). These results suggest that RBO is essential for stimulus-induced production of endosomal-like cisternae.

The FM-dye-uptake defects reported above are presumably due to the loss of dye internalization specifically within these cisternae, produced by bulk endocytosis from the plasma membrane under conditions of intense demand (Heerssen et al., 2008; Teng et al., 2007). To test this hypothesis, we performed FM1-43-dye-uptake experiments, as above (Fig. 1), and then photoconverted the label into an electron-dense marker for viewing with electron microscopy (Fig. 10). In control synapses, recently endocytosed dye was observed in two locations: (1) small (<40-nm diameter) SVs (arrows in Fig. 10A, left) and (2) large (>60-nm diameter) endosomes (asterisk in Fig. 10A, left). By sharp contrast, *rbo*^{ts} synaptic boutons at 37°C showed all endocytosed FM dye in small SVs, with no dye being present in endosomes (Fig. 10A, right). We quantified the number of electron-dense labeled SVs (Fig. 10B) and endosomes (Fig. 10C). Following 10 minutes at 37°C with high-demand stimulation, *rbo*^{ts} boutons contained significantly more labeled SVs than controls (OR, 67.9±15.2; *rbo*^{ts}, 130.1±16.3; $P<0.01$) (Fig. 10B). Under the same conditions, *rbo*^{ts} boutons contained essentially no labeled endosomes, with only a couple examples observed among all the sections assayed. The result is a very highly significant ($P<0.0001$) loss of endosome production in the mutant (OR, 5.8±0.8; *rbo*^{ts}, 0.4±0.2) (Fig. 10C). Thus, RBO is specifically required for endosome formation at the synapse.

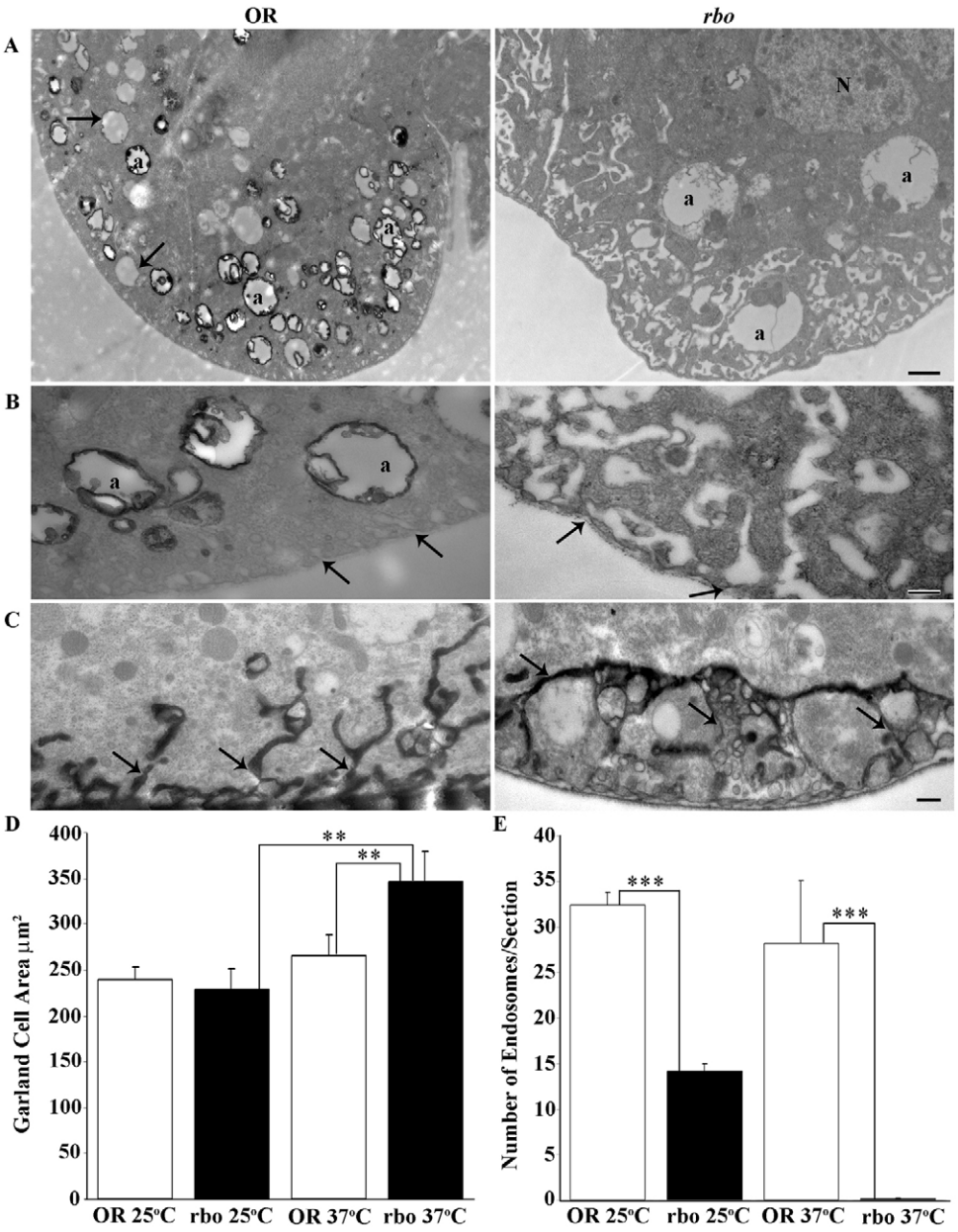

Fig. 8. Block in HRP endocytosis occurs in Garland cells in the absence of RBO. (A) Garland-cell endocytotic activity visualized using HRP uptake in wild type (OR) and *rbo*^{ts} after 10 minutes at 37°C. Many coated profiles of α vacuoles (a) are labeled in wild type (left), among pre-existing unlabeled α vacuoles (arrows). The mutant (right) shows no HRP uptake into α vacuoles (a). N, nucleus. Scale bar: 1 µm. (B) Higher-magnification images of α vacuoles (a) and labyrinthine channels (arrows). The mutant (right) shows an absence of labeling, with distended and swollen labyrinthine channels. Scale bar: 250 nm. (C) Tannic-acid impregnation shows labyrinthine channels that are continuous with the extracellular space. In *rbo*^{ts}, the channels are fused with many vacuolar inclusions. Scale bar: 250 nm. (D) Quantification of cell area. No change was observed in *rbo*^{ts} at 25°C compared with wild type, but a highly significant increase in cell area was seen at 37°C. (E) Quantification of loaded endosomes per section. A significant reduction in the number of loaded endosomes was observed in *rbo*^{ts} at 25°C compared with wild type, with near complete loss at 37°C.

Discussion

The conditional *rolling blackout* mutant (*rbo*^{ts}) paralyzes within minutes at 37°C (Huang et al., 2006). Of numerous double-mutant combinations with other TS paralytic mutants, *rbo*^{ts} displays a unique synergistic interaction with the t-SNARE Syntaxin-1A allele *syx*$^{3\text{-}69}$. We therefore hypothesized that RBO and Syntaxin-1A act together in SV exocytosis. However, recent re-evaluation of *syx*$^{3\text{-}69}$ forced us to radically reinterpret our previous conclusion. In the original paper (Littleton et al., 1998), the *syx*$^{3\text{-}69}$ T254I mutation was shown to block SV exocytosis because of a failure to form 7S SNARE complexes. In stark contrast, the new *syx*$^{3\text{-}69}$ study (Lagow et al., 2007) utterly contradicts the earlier report, showing that the mutant T-I substitution confers a dominant positive effect on Syntaxin-1A, promoting 7S-SNARE-complex formation and increasing SV fusion. This is not at all compatible with an additive defect with *rbo*^{ts} in blocking SV exocytosis. In evaluating this inconsistency, we found that *rbo*^{ts} has a temperature-dependent defect in FM1-43 endocytosis at the NMJ synapse, a defect that is fully rescued by reintroducing the wild-type *rbo* gene. Moreover, *rbo*^{ts};*syx*$^{3\text{-}69}$ double mutants displayed a severe synergistic defect in FM endocytosis at permissive temperature. These new results, together with those of Lagow et al. (Lagow et al., 2007) lead us to conclude that there is a requirement for RBO in endocytosis, which becomes more demanding in *rbo*^{ts};*syx*$^{3\text{-}69}$ double mutants owing to an increased need to recycle SVs to keep up with increased fusion rate.

This new conclusion would seem incompatible with our earlier analyses at the adult DLM synapse (Huang et al., 2006). Is it possible that RBO has different requirements at different places? Supporting this possibility is the fact that RBO is acutely required to maintain neurotransmission at the adult DLM synapse, with a *rbo*^{ts} block in <3 minutes, but shows no such role at the larval NMJ synapse, even

after *rbo*^{ts} is at the restrictive temperature for >30 minutes (Huang et al., 2006). To determine whether RBO function is stage-specific (larval vs adult), or synapse-specific (e.g. central vs peripheral), we performed FM assays on pupal central brain primary cultured neurons, which contain many classes of synapse (Campusano et al., 2007; Jiang et al., 2005; Su and O'Dowd, 2003). In central synapses, RBO clearly localized to synaptic varicosities, together with synaptic markers such as CSP, Synapsin and Bruchpilot. These RBO-positive varicosities were clearly presynaptic specializations, which took up and released FM dye in a depolarization-dependent manner. In *rbo*^{ts} neurons there was a clear, temperature-dependent requirement for RBO in endocytosis. Although some mutant synapses were able to load dye, and a few showed strong labeling, many failed to load any dye at detectable levels. Overall, there was a highly significant reduction in FM endocytosis in *rbo*^{ts} synapses, strongly supporting a conserved endocytosis function for RBO in different developmental stages and classes of synapse. Nevertheless, the fact that some *rbo*^{ts} neurons showed comparatively normal FM-dye cycling and others showed none might signify that some neuron classes are more sensitive to disruption of RBO function. This is the first study ever to perform FM assays in a brain culture system or analyze genetic mutants in culture in the *Drosophila* system. Thus, these analyses represent a significant technical advance.

To dissect the endocytic RBO mechanism, we first turned to the large, accessible Garland cells, which maintain a high, constitutive rate of vesicular endocytosis (Kosaka and Ikeda, 1983; Narita et al., 1989). In *rbo*^{ts} cells, there was a severe decrease in Texas-red-conjugated avidin uptake, just as the synapse shows a decrease in FM-dye uptake. Ultrastructural analysis reveals a dramatic enlargement and vacuolization of plasma-membrane labyrinthine channels and loss of endosomes. Use of HRP as an endocytic tracer revealed a defect of plasma-membrane endocytosis into endosomes. Formation of tracer-labeled endosomes was already somewhat impaired at 25°C and was blocked at the 37°C restrictive temperature. A similar block in uptake was observed in the *shibire*^{ts} Dynamin mutant, consistent with a similar endocytic defect (Lloyd et al., 2002; Narita et al., 1989). Moreover, enlarged α vacuoles appeared in *rbo*^{ts} cells, similar to the phenotype of the hepatocyte growth factor-regulated tyrosine kinase substrate (HRS) mutant (Lloyd et al., 2002), which is defective in endosomal membrane invagination. On the basis of ultrastructural analyses, RBO function appears to be required for membrane curvature and/or budding during this endocytic mechanism, prior to Dynamin function.

In several neuronal systems, strong stimulation drives the formation of endosomes, taken in from the plasma membrane by an activity-dependent bulk endocytosis (Holt et al., 2003; Royle and Lagnado, 2003). In synaptosomal preparations and cultured hippocampal neurons, fluid-phase tracers such as HRP localize to these structures, showing that they are an immediate product of the synaptic-terminal-surface endosomal system (Leenders et al., 2002; Takei et al., 1996). In the *Drosophila* NMJ synapse, high-[K^+] depolarization for just 10 minutes caused a nearly fourfold increase in the number of these endosomes. Their formation was totally blocked in *rbo*^{ts} at 37°C, revealing an absolute RBO requirement in activity-dependent endosome formation. Because no SV depletion was observed in these mutants, this suggests that RBO is specifically required in the endosome-formation pathway. The best means of testing this hypothesis was to determine whether acutely endocytosed FM dye localizes to these structures, and whether this uptake is specifically blocked in the acute absence of RBO function. We therefore performed FM1-43-dye labeling for just 2 minutes

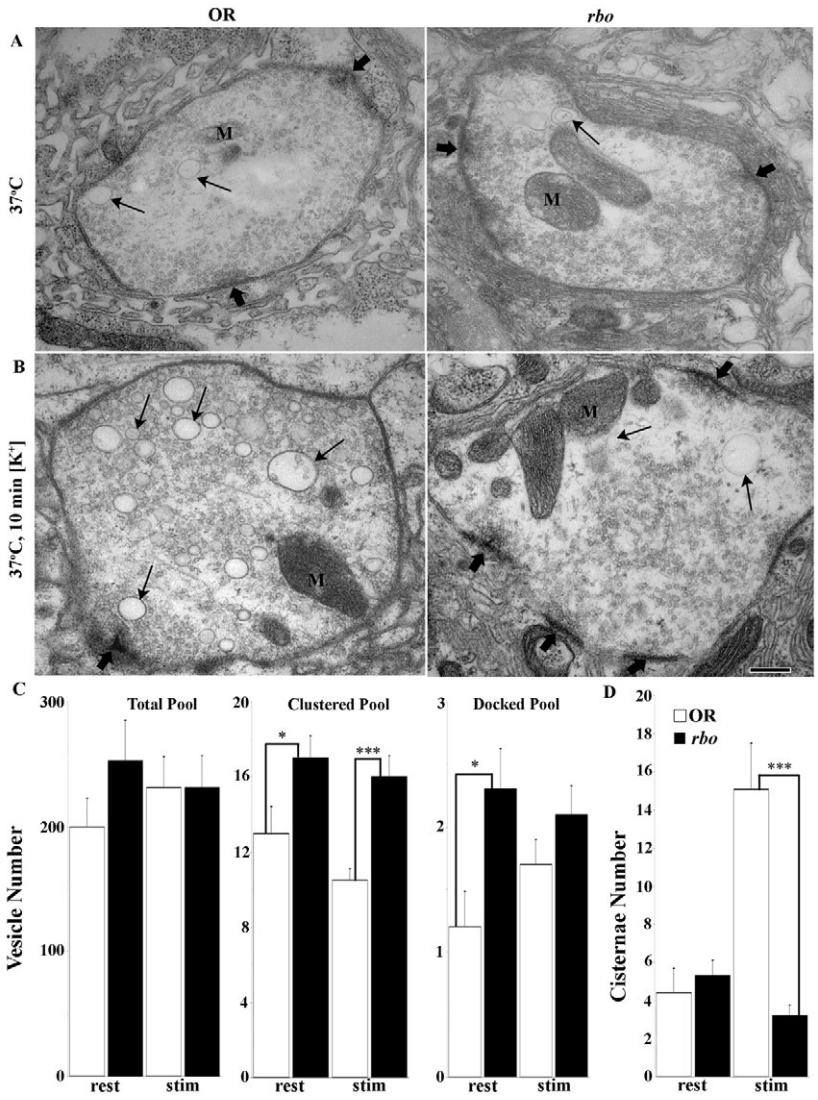

Fig. 9. RBO function is specific for bulk endocytosis in neuromuscular synapses. (A) Wild type (OR) and *rbo*^{ts} after 10 minutes at 37°C display similar NMJ synaptic ultrastructures. Boutons contain plentiful SVs, especially clustered near active zones (thick arrows), many mitochondria (M) and a few larger (>60 nm) cisternae (thin arrows). (B) Terminals challenged for 10 minutes with depolarizing 60 mM [K^+] saline show activity-dependent changes. In wild type (left), the primary ultrastructure change is a massive production of cisternae (thin arrows). In *rbo*^{ts} (right), new cisternae conspicuously fail to form. Scale bar: 250 nm. (C) Quantification of SV number in conditions of rest and high-[K^+] stimulation (stim). (D) The number of cisternae (>60 nm in diameter) is the same at rest, but very significantly increased by activity in wild type only.

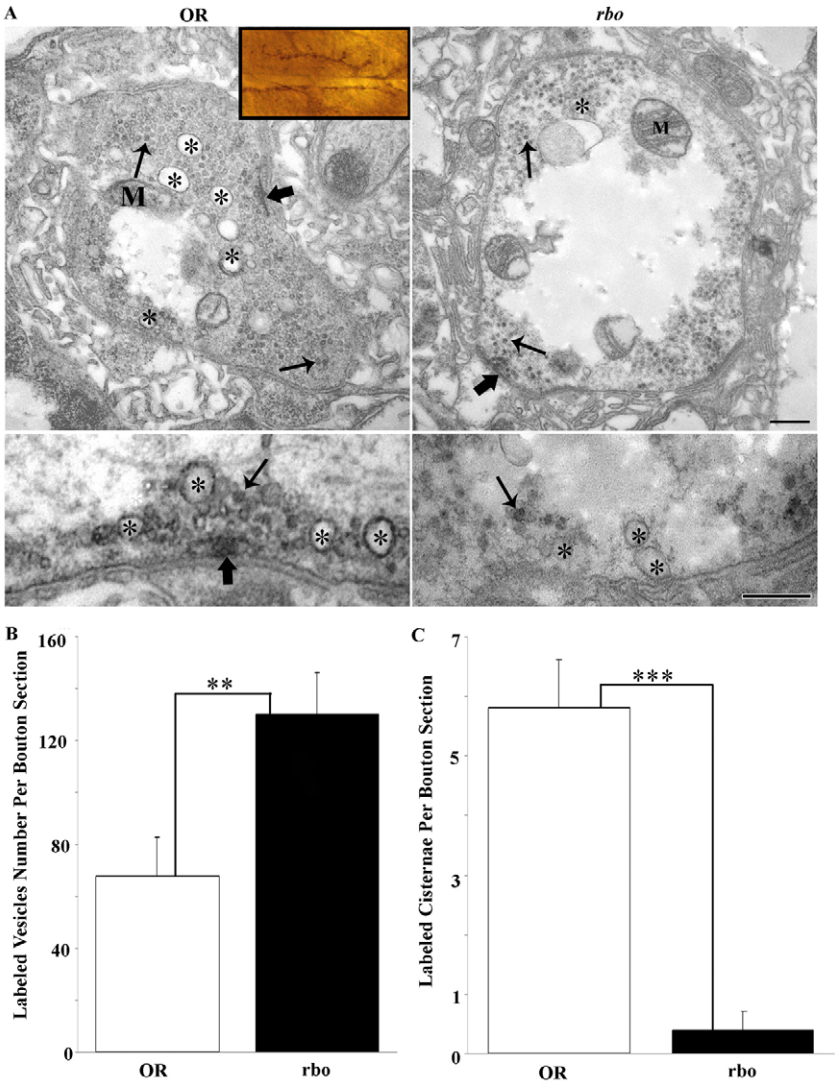

Fig. 10. RBO is required for activity-dependent endosome formation in synapses. FM1-43 photoconversion generates an electron-dense marker that is clearly visible by electron microscopy. Dye was incorporated into NMJ synapses after a 2-minute high-[K^+] stimulation at 37°C, photoconverted and examined in wild type (OR) and *rbo*^{ts}. (A) Inset shows a light-microscopy image of muscle 6/7 NMJ as photoconverted, ready to be sectioned at the electron-microscopic level. Top panels show representative images of control and mutant bouton profiles. Many FM-labeled vesicles and endosomes can be seen throughout the boutons. Asterisks (*) mark labeled endosomes in wild type; note the absence of label in *rbo*^{ts}. Lower panels show higher-magnification images of endosomes (*) and SVs (thin arrows). In *rbo*^{ts}, no labeling of endosomes was observed (*), but abundant SVs were labeled. Scale bars: 250 nm. (B) Quantification of FM-labeled SVs per bouton section. (C) Quantification of FM-labeled endosomes per bouton profile. Significance indicated: $^{**}P<0.01$, $^{***}P<0.001$.

with depolarizing high-[K^+] stimulation and then photoconverted the dye using photo-illumination with DAB to visualize the internalized dye ultrastructurally (Harata et al., 2001; Schikorski and Stevens, 2001). To our knowledge, this powerful technique has never before been used in *Drosophila*. Dye was observed in small SVs that were internalized by CME, in both controls and *rbo*^{ts} mutants, indicating that CME is not dependent on RBO function. By contrast, internalized dye was clearly observed in the enlarged endosomes in wild-type synapses, but is effectively never observed in *rbo*^{ts} synapses. This argues that endosomes are formed by direct uptake from the plasma membrane during strong stimulation and that this form of uptake is specifically disrupted in the absence of RBO. Interestingly, dye that was internalized by CME in *rbo*^{ts} was exocytosed, whereas dye that is internalized by bulk endocytosis following clathrin inactivation is not re-released (Heerssen et al., 2008). One model is that bulk endocytosis is totally RBO-dependent, but direct CME of SVs does not require RBO. In this model, a presumed increased rate of CME endocytosis is a compensatory response to the loss of bulk endocytosis in the absence of RBO function. An alternative model is that vesicles that are internalized by CME fail to fuse to form endosomes, because the fusion step requires RBO. In this model, the accumulation of small vesicles in *rbo*^{ts} mutants would represent an arrest in the endosomal formation pathway following endocytosis.

Contrary to expectations, *rbo*^{ts} synapses actually showed a higher SV density than controls, even after 20 minutes at restrictive temperature. We previously reported a similar phenotype at the adult DLM synapse (Huang et al., 2006). In both larval and adult synapses, there was an increase in clustered and/or docked vesicle pools at the active zone, a phenotype always interpreted as an exocytosis block. However, it has been suggested that SV endocytosis and exocytosis can both occur at the active zone (Koenig and Ikeda, 1999; Koenig et al., 1998), so it is possible that SVs accumulated at this location also represent a defect in SV fission or maturation. Consistent with this idea, we clearly observed photoconverted FM dye in vesicles under the T-bar active zone. However, given the limited temporal resolution with our 2-minute loading protocol, it is possible that these vesicles were already docked ready to undergo exocytosis (e.g. assuming a SV cycle of <30 seconds). Note also that FM assays showed comparable levels of SV exocytosis in *rbo*^{ts} and *syx*$^{3\text{-}69}$ mutants relative to wild-type controls. How does a synapse maintain exocytosis with impaired endocytosis in the absence of RBO function? Why are SVs not depleted, but actually slightly accumulated in the mutant synapse? The reason presumably

is that bulk retrieval plays only a small facilitatory role in acute synaptic function, as has been established at the *Drosophila* NMJ (Heerssen et al., 2008). Indeed, direct CME of SVs appeared enhanced in *rbo*^{ts} and might partially compensate for loss of SVs from the RBO-dependent endosomal pathway. These results suggest a delicate balance between CME and bulk-endocytosis mechanisms under conditions of high demand, and possibly the ability for crosstalk among different endocytosis mechanisms.

Our previous work has shown that RBO functions in PLC-dependent PtdIns(4,5)P_2-DAG signaling (Huang et al., 2004). Consistently, the local turnover of phosphoinositides by PLC and PI3-kinase activities has been suggested to regulate membrane curvature and related processes during bulk-membrane endocytosis (Araki et al., 2006). We have proposed that RBO might modify PtdIns(4,5)P_2 acyl side chains, making it inaccessible to subsequent conversion to other phospholipid species, which may in turn be required for bulk endocytosis. RBO is thus hypothesized to synthesize or locally concentrate phospholipid species at foci, mediating nucleation of membrane retrieval. An alternative model is that endocytic defects could be due to decreased DAG levels in *rbo*^{ts} mutants (Huang et al., 2004). DAG regulates ADP ribosylation factor (ARF) in vesicle budding (Antonny et al., 1997). DAG also activates PKC, UNC-13, RasGrp and chimaerins (Yang and Kazanietz, 2003). DAG kinase δ (DGKδ), which converts DAG to phosphatidic acid, has also been implicated in plasma-membrane endocytosis (Kawasaki et al., 2008). In the absence of RBO function, these lipids might be absent or aberrantly distributed in the plasma membrane and therefore unable to trigger membrane invagination. Our on-going studies are aimed at addressing the mechanistic interaction between RBO and phospholipids and/or DAG in the plasma membrane.

Materials and Methods

Drosophila stocks

Drosophila stocks were maintained on standard food under standard rearing conditions at 25°C. Animals were shifted between permissive (25°C) and restrictive (37°C) temperatures as indicated in individual experiments. Oregon-R (OR) was used as the wild-type control. The *rbo*^{2} allele is a null, the TS allele *rbo*^{ts} contains a G487D missense mutation, and *rbo-egfp* is driven by the native *rbo* promoter in the *rbo*^{2} background (Huang et al., 2004; Huang et al., 2006). The *syntaxin*$^{3\text{-}69}$ (T254I) (Lagow et al., 2007; Littleton et al., 1998) and *shibire*^{ts} (van der Bliek and Meyerowitz, 1991) lines were provided by Barry Ganetzky, University of Wisconsin, Madison, WI.

Immunocytochemistry

RBO-eGFP imaging was performed on *rbo*^{2}/*rbo*^{2}; *rbo-egfp/rbo-egfp* transgenic rescue animals (Huang et al., 2004; Huang et al., 2006). Coverslips were fixed in 4% paraformaldehyde for 30 minutes, washed three times in PBS with 0.1% Triton-X (PBS-TX) and blocked in PBS-TX containing 2.5% BSA for 1 hour. The following antibodies were used overnight at 4°C: anti-GFP 5450 (1:250, goat, Abcam), anti-Synapsin (Syn; 1:100 mouse, DSHB), anti-Bruchpilot (BRP; 1:100, mouse, provided by Hugo Bellen, Baylor College of Medicine, Houston, TX) and anti-CSP (1:200, mouse, provided by Konrad Zinsmaier, University of Arizona, Tucson, AZ). Secondary antibodies conjugated to TritC or Alexa-Fluor-488 were used at 1:250 (Jackson Immunolabs, Molecular Probes). Images were captured with a Zeiss 510 Meta confocal microscope and processed with Adobe Photoshop CS8.

FM-dye imaging assays

FM1-43-dye loading and unloading assays were performed on wandering third instar NMJ as previously described (Fergestad and Broadie, 2001). Briefly, FM1-43 dye (10 μM; Molecular Probes, Eugene, OR) was applied in 60 mM depolarizing K^+ saline in 1.8 mM Ca^{2+} for 2 minutes at 25°C. Preparations were subsequently washed in Ca^{2+}-free saline before imaging. For restrictive-temperature experiments, preparations were incubated for 10 minutes at 37°C and then a 2-minute pulse of FM1-43 dye was applied in 60 mM K^+ saline. Samples were then washed at 37°C in Ca^{2+}-free saline and imaged. To assay exocytosis, loaded terminals were stimulated for 2 minutes with 60 mM K^+ saline, either at 25°C or 37°C. Equidistant confocal slices were scanned from muscle 6/7 NMJs, four NMJs per animal, two each from segments A3 and A4. Quantification was done using ImageJ (NIH), with average pixel intensity for the entire *z*-stack 3D bouton determined. Mean pixel intensity was calculated for ten boutons per NMJ and averaged across each animal (n = number of animals). Pupal neurons were cultured based on the protocol described by Jiang et al. (Jiang et al., 2005). Cultures at 5-8 days were incubated with FM1-43 dye for 45 seconds, either at 25°C or following 10 minutes at 37°C. Synapse fields were selected using DIC optics, with 20 fields imaged per coverslip. For quantification, the total number of DIC punctae and number of dye-loaded punctae were each counted per 20-μm distance of axonal processes using LSM software (n = number of coverslips). A 63×, 0.95W water-immersion objective on a Zeiss LSM 510 confocal microscope was used for image acquisition.

Garland-cell tracer-endocytosis assays

Endocytic tracer assays were performed on Garland cells as described (Dermaut et al., 2005). Briefly, Garland cells were dissected from wandering third instars in Schneider's culture medium (Gibco) and incubated at 25°C or 37°C for 10 minutes. Texas-red-conjugated avidin (0.2 mg/ml; Sigma Aldrich) was applied for 5 minutes, followed by fixation with 4% paraformaldehyde for 15 minutes. Quantification of tracer uptake was done using ImageJ (NIH). An outline of the cell was drawn and total fluorescence-intensity measured. A second circle was similarly drawn in the cell interior. Subtracting this value from the whole-cell value generated the peri-membrane fluorescence. Imaging was done using a Zeiss LSM 510 Meta confocal microscope.

Electron microscopy

Analyses of NMJ-synapse and Garland-cell ultrastructures were performed as reported previously (Pan et al., 2004; Rohrbough et al., 2007). Briefly, for stimulated and unstimulated assays, dissected wandering third instars were incubated at 37°C in 60 mM K^+ saline with 1.8 mM Ca^{2+} or Ca^{2+}-free saline, respectively. Specimens were fixed in 2% glutaraldehyde for 1 hour, washed in PBS for 10 minutes and transferred into 1% OsO_4 in dH_20 for 1 hour. Preparations were stained en bloc in 1% aqueous uranyl acetate for 1 hour, dehydrated using a graded series of ethanol followed by propylene oxide for 30 minutes and then embedded in araldite. Ultrathin (<60 nm) sections were obtained using a Leica Ultracut UCT 54 ultramicrotome and were transferred to formvar-coated slot grids placed on Synaptiek grid-sticks to be blocked stained with lead nitrate and uranyl acetate. Sections were imaged using a Phillips CM10 TEM at 80V with images from a 2-megapixel AMT CCD camera.

TA-impregnation and HRP-uptake methods

Following the method of Kosaka and Ikeda (Kosaka and Ikeda, 1983), TA was used to mark internalized lumens continuous to the extracellular space. After the osmification step in the transmission electron microscopy methods above, specimens were rinsed twice for 5 minutes with 1% TA and then immersed for 1 hour with agitation at room temperature. HRP in modified Bodenstein saline (0.7% HRP solution) was used to assay endocytotic activity in Garland cells (Kosaka and Ikeda, 1983). Garland cells were incubated in HRP solution for 10 minutes, either at 25°C or 37°C. The cells were then fixed in 1.6% paraformaldehyde, 2% glutaraldehyde in PBS for 20 minutes. Samples were rinsed overnight in 0.1 M phosphate buffer at 4°C and then incubated in 0.15% 3,3′-diaminobenzidine (DAB, DEKO) for 20 minutes at room temperature. All samples were further processed for electron microscopy using the standard protocol, as described above.

FM1-43 photoconversion

FM1-43 dye loading was done as described above and then preparations were fixed for 5 minutes in 1.6% paraformaldehyde/2% glutaraldehyde in PBS. Samples were washed for 20 minutes in Tris-buffered saline (TBS, pH 7.5) and then incubated in 0.15% 3,3′-diaminobenzidine (DAB, DEKO) in TBS for 5 minutes. The DAB solution was refreshed and samples were then illuminated using a 100 W mercury lamp, a 63× 0.95W objective and a standard FITC filter for 20 minutes. The photoconverted samples (see Fig. 10A, inset) were post-fixed overnight in 2% glutaraldehyde at 4°C. Samples were placed in osmium (1% OsO_4) at room temperature for 30 minutes, washed and then placed in uranyl acetate at room temperature for 30 minutes. Samples were dehydrated through ethanol and then propylene oxide for 30 minutes, placed in a 1:1 ratio of propylene oxide and Spurr's resin for 30 minutes and finally for 1 hour in pure resin in a vacuum oven. Samples were taken out and further dissected so that only muscles 6 and 7 were embedded for thin sectioning. Ultrathin (<60 nm) sections were cut on a Leica ultra cut UCT microtome. Samples were then processed for electron microscopy using the standard protocol, as described above.

We are indebted to Thomas Schikorski for guidance on FM dye photoconversion techniques. We are grateful to Cheryl Gatto for guidance on primary neuron cultures, and Diane O'Dowd for sharing culturing expertise with our laboratory. We thank Barry Ganetzky, Konrad Zinsmaier and Hugo Bellen for providing *Drosophila* stocks and antibodies. We gratefully acknowledge the Bloomington *Drosophila* Stock Center and the Developmental Studies Hybridoma Bank (DSHB) at the University of Iowa for crucial reagents. This work was supported by NIH grants NS41740 and GM54544 to K.B. Deposited in PMC for release after 12 months.

References

Antonny, B., Huber, I., Paris, S., Chabre, M. and Cassel, D. (1997). Activation of ADP-ribosylation factor 1 GTPase-activating protein by phosphatidylcholine-derived diacylglycerols. *J. Biol. Chem.* **272**, 30848-30851.

Araki, N., Hamasaki, M., Egami, Y. and Hatae, T. (2006). Effect of 3-methyladenine on the fusion process of macropinosomes in EGF-stimulated A431 cells. *Cell Struct. Funct.* **31**, 145-157.

Beramendi, A., Peron, S., Casanova, G., Reggiani, C. and Cantera, R. (2007). Neuromuscular junction in abdominal muscles of Drosophila melanogaster during adulthood and aging. *J. Comp. Neurol.* **501**, 498-508.

Campusano, J. M., Su, H., Jiang, S. A., Sicaeros, B. and O'Dowd, D. K. (2007). nAChR-mediated calcium responses and plasticity in Drosophila Kenyon cells. *Dev. Neurobiol.* **67**, 1520-1532.

Chang, H. C., Newmyer, S. L., Hull, M. J., Ebersold, M., Schmid, S. L. and Mellman, I. (2002). Hsc70 is required for endocytosis and clathrin function in Drosophila. *J. Cell Biol.* **159**, 477-487.

de Lange, R. P., de Roos, A. D. and Borst, J. G. (2003). Two modes of vesicle recycling in the rat calyx of Held. *J. Neurosci.* **23**, 10164-10173.

Dermaut, B., Norga, K. K., Kania, A., Verstreken, P., Pan, H., Zhou, Y., Callaerts, P. and Bellen, H. J. (2005). Aberrant lysosomal carbohydrate storage accompanies endocytic defects and neurodegeneration in Drosophila benchwarmer. *J. Cell Biol.* **170**, 127-139.

Fergestad, T. and Broadie, K. (2001). Interaction of stoned and synaptotagmin in synaptic vesicle endocytosis. *J. Neurosci.* **21**, 1218-1227.

Gonzalez-Gaitan, M. and Jackle, H. (1997). Role of Drosophila alpha-adaptin in presynaptic vesicle recycling. *Cell* **88**, 767-776.

Harata, N., Ryan, T. A., Smith, S. J., Buchanan, J. and Tsien, R. W. (2001). Visualizing recycling synaptic vesicles in hippocampal neurons by FM 1-43 photoconversion. *Proc. Natl. Acad. Sci. USA* **98**, 12748-12753.

Heerssen, H., Fetter, R. D. and Davis, G. W. (2008). Clathrin dependence of synaptic-vesicle formation at the Drosophila neuromuscular junction. *Curr. Biol.* **18**, 401-409.

Heuser, J. E. and Reese, T. S. (1973). Evidence for recycling of synaptic vesicle membrane during transmitter release at the frog neuromuscular junction. *J. Cell Biol.* **57**, 315-344.

Hinshaw, J. E. (2000). Dynamin and its role in membrane fission. *Annu. Rev. Cell Dev. Biol.* **16**, 483-519.

Holt, M., Cooke, A., Wu, M. M. and Lagnado, L. (2003). Bulk membrane retrieval in the synaptic terminal of retinal bipolar cells. *J. Neurosci.* **23**, 1329-1339.

Huang, F. D., Matthies, H. J., Speese, S. D., Smith, M. A. and Broadie, K. (2004). Rolling blackout, a newly identified PIP2-DAG pathway lipase required for Drosophila phototransduction. *Nat. Neurosci.* **7**, 1070-1078.

Huang, F. D., Woodruff, E., Mohrmann, R. and Broadie, K. (2006). Rolling blackout is required for synaptic vesicle exocytosis. *J. Neurosci.* **26**, 2369-2379.

Jiang, S. A., Campusano, J. M., Su, H. and O'Dowd, D. K. (2005). Drosophila mushroom body Kenyon cells generate spontaneous calcium transients mediated by PLTX-sensitive calcium channels. *J. Neurophysiol.* **94**, 491-500.

Kawasaki, T., Kobayashi, T., Ueyama, T., Shirai, Y. and Saito, N. (2008). Regulation of clathrin-dependent endocytosis by diacylglycerol kinase delta: importance of kinase activity and binding to AP2alpha. *Biochem. J.* **409**, 471-479.

Koenig, J. H. and Ikeda, K. (1989). Disappearance and reformation of synaptic vesicle membrane upon transmitter release observed under reversible blockage of membrane retrieval. *J. Neurosci.* **9**, 3844-3860.

Koenig, J. H. and Ikeda, K. (1996). Synaptic vesicles have two distinct recycling pathways. *J. Cell Biol.* **135**, 797-808.

Koenig, J. H. and Ikeda, K. (1999). Contribution of active zone subpopulation of vesicles to evoked and spontaneous release. *J. Neurophysiol.* **81**, 1495-1505.

Koenig, J. H., Yamaoka, K. and Ikeda, K. (1998). Omega images at the active zone may be endocytotic rather than exocytotic: implications for the vesicle hypothesis of transmitter release. *Proc. Natl. Acad. Sci. USA* **95**, 12677-12682.

Kosaka, T. and Ikeda, K. (1983). Reversible blockage of membrane retrieval and endocytosis in the garland cell of the temperature-sensitive mutant of Drosophila melanogaster, shibirets1. *J. Cell Biol.* **97**, 499-507.

Kuppers-Munther, B., Letzkus, J. J., Luer, K., Technau, G., Schmidt, H. and Prokop, A. (2004). A new culturing strategy optimises Drosophila primary cell cultures for structural and functional analyses. *Dev. Biol.* **269**, 459-478.

Kuromi, H. and Kidokoro, Y. (1998). Two distinct pools of synaptic vesicles in single presynaptic boutons in a temperature-sensitive Drosophila mutant, shibire. *Neuron* **20**, 917-925.

Lagow, R. D., Bao, H., Cohen, E. N., Daniels, R. W., Zuzek, A., Williams, W. H., Macleod, G. T., Sutton, R. B. and Zhang, B. (2007). Modification of a hydrophobic layer by a point mutation in syntaxin 1A regulates the rate of synaptic vesicle fusion. *PLoS Biol.* **5**, e72.

Leenders, A. G., Scholten, G., de Lange, R. P., Lopes da Silva, F. H. and Ghijsen, W. E. (2002). Sequential changes in synaptic vesicle pools and endosome-like organelles during depolarization near the active zone of central nerve terminals. *Neuroscience* **109**, 195-206.

Littleton, J. T., Chapman, E. R., Kreber, R., Garment, M. B., Carlson, S. D. and Ganetzky, B. (1998). Temperature-sensitive paralytic mutations demonstrate that synaptic exocytosis requires SNARE complex assembly and disassembly. *Neuron* **21**, 401-413.

Lloyd, T. E., Atkinson, R., Wu, M. N., Zhou, Y., Pennetta, G. and Bellen, H. J. (2002). Hrs regulates endosome membrane invagination and tyrosine kinase receptor signaling in Drosophila. *Cell* **108**, 261-269.

Marxen, M., Volknandt, W. and Zimmermann, H. (1999). Endocytic vacuoles formed following a short pulse of K^+-stimulation contain a plethora of presynaptic membrane proteins. *Neuroscience* **94**, 985-996.

Narita, K., Tsuruhara, T., Koenig, J. H. and Ikeda, K. (1989). Membrane pinch-off and reinsertion observed in living cells of Drosophila. *J. Cell Physiol.* **141**, 383-391.

Neves, G., Gomis, A. and Lagnado, L. (2001). Calcium influx selects the fast mode of endocytosis in the synaptic terminal of retinal bipolar cells. *Proc. Natl. Acad. Sci. USA* **98**, 15282-15287.

Oh, H. W., Campusano, J. M., Hilgenberg, L. G., Sun, X., Smith, M. A. and O'Dowd, D. K. (2008). Ultrastructural analysis of chemical synapses and gap junctions between Drosophila brain neurons in culture. *Dev. Neurobiol.* **68**, 281-294.

Pan, L., Zhang, Y. Q., Woodruff, E. and Broadie, K. (2004). The Drosophila fragile X gene negatively regulates neuronal elaboration and synaptic differentiation. *Curr. Biol.* **14**, 1863-1870.

Poodry, C. A. and Edgar, L. (1979). Reversible alteration in the neuromuscular junctions of Drosophila melanogaster bearing a temperature-sensitive mutation, shibire. *J. Cell Biol.* **81**, 520-527.

Renden, R. B. and Broadie, K. (2003). Mutation and activation of Galpha s similarly alters pre- and postsynaptic mechanisms modulating neurotransmission. *J. Neurophysiol.* **89**, 2620-2638.

Richards, D. A., Guatimosim, C. and Betz, W. J. (2000). Two endocytic recycling routes selectively fill two vesicle pools in frog motor nerve terminals. *Neuron* **27**, 551-559.

Richards, D. A., Rizzoli, S. O. and Betz, W. J. (2004). Effects of wortmannin and latrunculin A on slow endocytosis at the frog neuromuscular junction. *J. Physiol.* **557**, 77-91.

Rohrbough, J., Rushton, E., Woodruff, E., 3rd, Fergestad, T., Vigneswaran, K. and Broadie, K. (2007). Presynaptic establishment of the synaptic cleft extracellular matrix is required for post-synaptic differentiation. *Genes Dev.* **21**, 2607-2628.

Royle, S. J. and Lagnado, L. (2003). Endocytosis at the synaptic terminal. *J. Physiol.* **553**, 345-355.

Schikorski, T. and Stevens, C. F. (2001). Morphological correlates of functionally defined synaptic vesicle populations. *Nat. Neurosci.* **4**, 391-395.

Slepnev, V. I. and De Camilli, P. (2000). Accessory factors in clathrin-dependent synaptic vesicle endocytosis. *Nat. Rev. Neurosci.* **1**, 161-172.

Su, H. and O'Dowd, D. K. (2003). Fast synaptic currents in Drosophila mushroom body Kenyon cells are mediated by alpha-bungarotoxin-sensitive nicotinic acetylcholine receptors and picrotoxin-sensitive GABA receptors. *J. Neurosci.* **23**, 9246-9253.

Takei, K., Mundigl, O., Daniell, L. and De Camilli, P. (1996). The synaptic vesicle cycle: a single vesicle budding step involving clathrin and dynamin. *J. Cell Biol.* **133**, 1237-1250.

Teng, H., Lin, M. Y. and Wilkinson, R. S. (2007). Macroendocytosis and endosome processing in snake motor boutons. *J. Physiol.* **582**, 243-262.

Trotta, N., Rodesch, C. K., Fergestad, T. and Broadie, K. (2004). Cellular bases of activity-dependent paralysis in Drosophila stress-sensitive mutants. *J. Neurobiol.* **60**, 328-347.

van der Bliek, A. M. and Meyerowitz, E. M. (1991). Dynamin-like protein encoded by the Drosophila shibire gene associated with vesicular traffic. *Nature* **351**, 411-414.

Verstreken, P., Koh, T. W., Schulze, K. L., Zhai, R. G., Hiesinger, P. R., Zhou, Y., Mehta, S. Q., Cao, Y., Roos, J. and Bellen, H. J. (2003). Synaptojanin is recruited by endophilin to promote synaptic vesicle uncoating. *Neuron* **40**, 733-748.

Vijayakrishnan, N. and Broadie, K. (2006). Temperature-sensitive paralytic mutants: insights into the synaptic vesicle cycle. *Biochem. Soc. Trans.* **34**, 81-87.

Wenk, M. R. and De Camilli, P. (2004). Protein-lipid interactions and phosphoinositide metabolism in membrane traffic: insights from vesicle recycling in nerve terminals. *Proc. Natl. Acad. Sci. USA* **101**, 8262-8269.

Yang, C. and Kazanietz, M. G. (2003). Divergence and complexities in DAG signaling: looking beyond PKC. *Trends Pharmacol. Sci.* **24**, 602-608.